Fabrication of 10 nm-Scale Complex 3D Nanopatterns with Multiple Shapes and Components by Secondary Sputtering Phenomenon

Hwan-Jin Jeon,[†,⊥] Hyeon Su Jeong,[‡,⊥] Yun Ho Kim,[§] Woo-Bin Jung,[†] Jeong Yeon Kim,[†] and Hee-Tae Jung*[,†]

[†]National Research Laboratory for Organic Opto-Electronic Materials, Department of Chemical and Biomolecular Engineering (BK-21), Korea Advanced Institute of Science and Technology, Daejeon 305-701, Korea, [‡]Optical Material Laboratory Materials R&D Center, SK Innovation, Yuseong-gu, Daejeon 305-712, Korea, and [§]Advanced Functional Materials Research Group, Korea Research Institute of Chemical Technology, 141 Gajeong-ro, Yuseong-gu, Daejeon 305-600, Korea. [⊥]H.-J.J. and H.S.J. contributed equally to this work.

ABSTRACT We introduce an advanced ultrahigh-resolution (~15 nm) patterning technique that enables the fabrication of various 3D high aspect ratio multicomponents/shaped nanostructures. This methodology utilizes the repetitive secondary sputtering phenomenon under etching plasma conditions and prepatterned fabrication control. The secondary sputtering phenomenon repetitively generates an angular distribution of target particles during ion-bombardment. This method, advanced repetitive secondary sputtering lithography, provides many strategies to fabricate complex continuous patterns and multilayer/material patterns with 10 nm-scale resolution. To demonstrate the versatility of this method, we show induced vertical alignment of liquid crystals (LCs) on indium-tin-oxide (ITO) grid patterns without any alignment layers. The ITO grid pattern fabricated in this method is found to have not only an alignment capability but also electrode properties without electrical or optical damage.

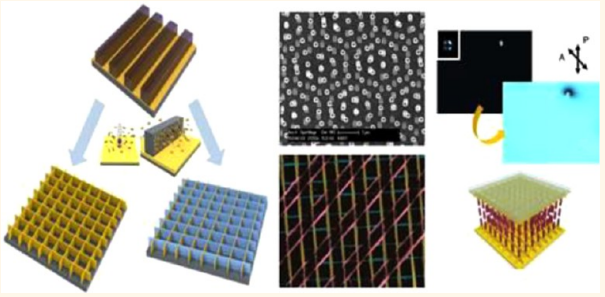

KEYWORDS: nanopattern · lithography · secondary sputtering · liquid crystal

The development of ~10 nm-scale three-dimensional (3D) nanostructures over large areas is one of the most important challenges in nanobiotechnology and opto-electronics due to the electric/optical peculiarities of different nanosized structures and material specificity.[1−11] High precise 10 nm-scale nanostructures with different shapes enable tunable electronic/optical devices that can control the intrinsic properties of target materials by changing the structure and size. Several approaches, which include nanoimprint,[12,13] soft-,[14] edge-,[15−18] colloidal-,[19] interference lithography,[20] the nanoskiving method,[21] electrodeposition,[22] and focused ion-beam (FIB)[23] and electron-beam[24] assisted deposition, have been suggested to fabricate 3D 10 nm-scale features. Recently, we introduced a new nanopatterning technique named "secondary sputtering lithography" (SSL),[25−27] which enables the fabrication of 10 nm-scale 3D patterned nanostructures with high aspect ratios over large areas by utilizing secondary sputtering phenomena during ion-bombardment. Secondary sputtering phenomena entail particles of target material being etched and emitted by accelerated Ar ions over a large angular distribution. We have fabricated many patterns on a 10 nm-scale, including lines, hole-cylinders, cups, and triangular tunnels. We have also applied ~10 nm-scale line patterns with a high aspect ratio to align liquid crystal molecules. High-resolution patterning (~20 nm) of indium-tin-oxide (ITO) surface layers with a high aspect ratio (~10) was successfully carried out without damage to the electrical/optical properties of the ITO, and the patterned ITO could function as a bifunctional conductive alignment layer for liquid crystal devices without a conventional polymer alignment layer fabrication process.

* Address correspondence to heetae@kaist.ac.kr.

Received for review July 22, 2013 and accepted January 9, 2014.

Published online January 09, 2014
10.1021/nn4037688

© 2014 American Chemical Society

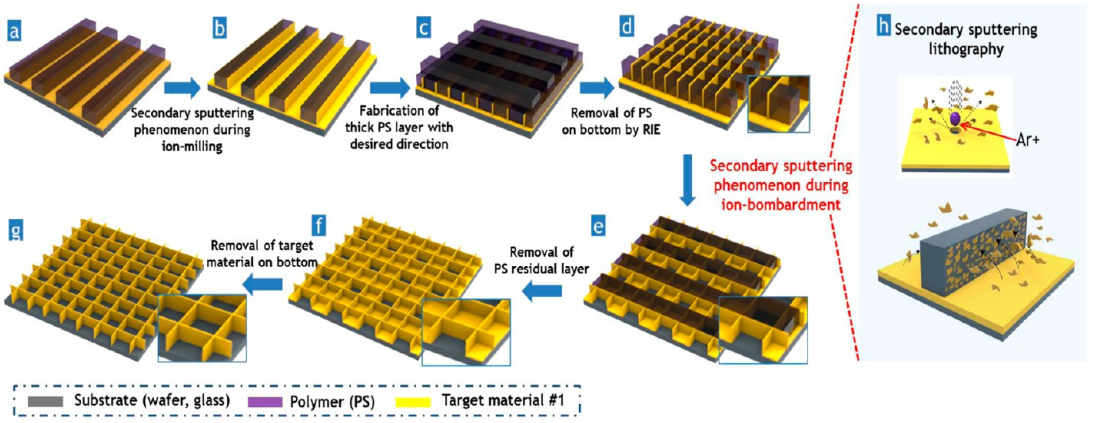

Figure 1. Schematic illustration of the overall fabrication of high resolution (~20 nm) complex 3D pattern by repetitive secondary sputtering phenomenon (a–g) and representative images of the secondary sputtering lithography (SSL) technique (h). (a) PS prepattern is fabricated on the target material deposited substrate from the PDMS mold and (b) secondary sputtered particles are attached to the side surface of prepattern. (c) A thick PS layer is spin-coated on the fabricated line patterned substrate, and (d) the PS layer that remains on the bottom is removed by RIE. (e) Again, the particles of target materials are attached on the side surface of the prepattern by SSL. (f) The PS prepattern is removed entirely by RIE. (g) Only a grid shaped pattern is generated by more etching.

In the studies described below, we made technologically significant advances to our secondary sputtering techniques: (i) We fabricated various ~10 nm scale multidirectional complex patterns, such as grids and connected Olympic ring-shaped hole-cylinders using single line and single pillar shape master patterns by a multistep SSL technique. (ii) We show that such ~10 nm scale grid patterns can enable the homeotropic alignment (vertical alignment) of liquid crystal molecules. Homeotropic alignment of LC molecules has been spotlighted recently for use in liquid crystal display (LCD) devices due to the possibility of high contrast and wide viewing angles, and polar angle (the angle between the optic axis of LCs and the *z*-axis) control of LC molecules is becoming more important for LC-based future nanodevices.[28−30] In addition, alignment using physical geometric nanostructures is considered a core technology for next-generation display devices, since the physical/chemical/thermal stability is high compared to a conventional chemical method of alignment. (iii) Furthermore ~10 nm scale multicomponent patterns, consisting of two or more kinds of material arranged alternately in some direction, can be fabricated using repetitive secondary sputtering lithography. This is very important for potential application in sensors, wave-guides, and microelectromechanical systems (MEMS), because one can obtain a versatile circuit element through the simultaneous use of the unique chemical, optical, and electrical properties of each component.

RESULTS AND DISCUSSION

Figure 1 displays a schematic illustration of the fabrication procedure for a ~10 nm scale, large-area, gold grid, and multicomponent nanopattern which was fabricated using our multistep secondary sputtering approach. Various types of metal or semiconductor templates can be prepared, provided that the different target layers can be deposited onto a substrate. First, a highly uniform gold layer (~40 nm thick, target material) was deposited using electron beam evaporation onto a substrate coated with a ~3 nm thick chromium adhesion layer. After spin-coating polystyrene [PS (18 000 g/mol)], a PS prepattern with 500 nm width is created by pattern-transfer using a PDMS mold (Figure 1a). A gold line pattern with 15 nm width and 500 nm spacing is fabricated on the side surface of the prepattern using secondary sputtering during ion-bombardment (Figure 1b, see Figures S1 and S2). Secondary sputtering lithography utilizes the secondary sputtering of particles of target materials, emitted with a large angular distribution *via* accelerated Ar^+ ion bombardment (Figure 1h). The gold line patterned substrate is spin-coated with 100 nm thick polystyrene [PS (18 000 g/mol)] to prepare the fabrication of another SSL pattern, in which the PS is thick enough to cover all of prefabricated gold line pattern. Then a PDMS mold with topographic features is placed onto the PS film perpendicular to the initial line pattern. After heating at 135 °C for 60 min followed by cooling to room temperature, the mold is removed from the surface (Figure 1c). The thick PS layer that remains on the bottom of the imprinted structure is etched until the gold substrate is exposed to a high vacuum reactive ion etching (RIE) plasma that has decreased isotropic etching compared to low vacuum RIE (Figure 1d). The gold layer was then etched and deposited simultaneously onto the side surface of the PS pattern by secondary sputtering during ion bombardment, and ~15 nm gold nanopatterns were formed on the side surface of the PS pattern (Figure 1e). This SSL line pattern was interconnected with the initial fabricated line pattern in the same plane (Figure 1e). The line pattern fabricated during the

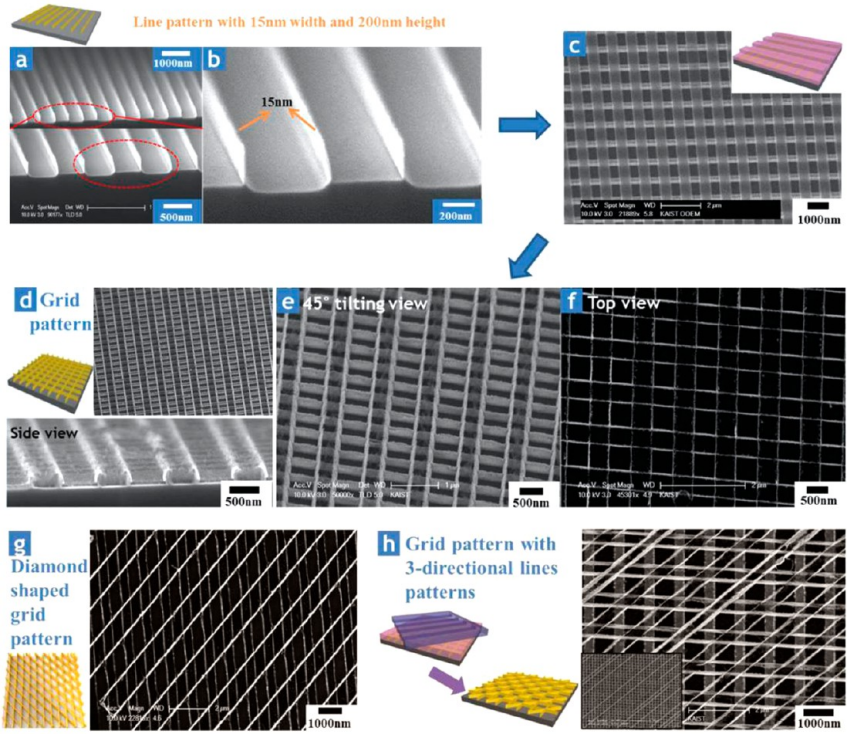

Figure 2. SEM images for fabrication of various representative gold grid patterns with high resolution (sub 20 nm) from a line shaped pattern master with 500 nm width and 500 nm spacing by repetitive SSL of 15 nm single line patterns. (a,b) Ultrathin gold line pattern with 15 nm width and 500 nm spacing fabricated by SSL over a large area and (c) PS line pattern with 500 nm width and spacing fabricated in the direction perpendicular to the initial line pattern. (d−f) SEM images of gold grid patterns including crossed two line patterns with 15 nm width in side view (d,e) and top view (f). (g) Grid pattern including two directional line patterns overlapped at 45°. (h) 3-directional gold grid pattern formed by 3 applications of the SSL method.

second process does not stack onto the initial line pattern. After the PS residual layer in the gold pattern is clearly removed by RIE, a ~15 nm grid-shaped gold pattern is fabricated on the square-shaped gold bottom layer (Figure 1f). Finally, a grid-shaped gold pattern is achieved over a large area after removal of the gold bottom layer (Figure 1g). It is noteworthy that multigrid patterns with different angles could be also obtained by simply rotating the PS line pattern during the second SSL process. In addition, a multicomponent (or multilayered) pattern, consisting of two or more kinds of materials arranged alternately in different directions, can be fabricated by simply varying the target materials deposited on the PS pattern (Supporting Information Figure S6). We believe that our method is a powerful tool to fabricate complex 3D patterns composed of multiple shapes, sizes, components, and layers.

Figure 2 shows scanning electron microscope (SEM) images of various Au grid patterns over large areas (macroscopic dimensions of several square centimeters) formed by the multistep secondary sputtering lithography (SSL) procedure. The patterned gold line is highly periodic with 15 nm width, 150 nm height, and 500 nm spacing (Figure 2a,b). The height and spacing are determined by the prepattern size of the PDMS mold, and the height of the gold line pattern was up to 300 nm while the width was ~15 nm. A thick PS layer was spin-coated again onto the patterned gold line substrate for the second SSL line pattern process. The thick PS residual layer remaining on the bottom could be etched by high vacuum RIE, revealing that the PS line pattern was crossed with respect to the initial gold line pattern on the same plane (Figure 2c). After ion-bombardment (ion-milling) and RIE, gold grid patterns featuring crossed lines with 15 nm width were created in the same plane by a double-step SSL technique (Figure 2d−f). The cross-sectional image in Figure 2c shows that the two-directional gold lines intersect each other and have 15 nm width, 250 nm height, and 500 nm spacing. A number of 15 nm gold walls can be clearly seen from a tilted SEM image (45°) due to the considerable height of the line pattern (Figure 2e), whereas the grid pattern looks so thin in a top-view since it has ~15 nm width and a relatively wide spacing of 500 nm (Figure 2f). Further, multigrid patterns with different angles could be also obtained by simply rotating the PS line pattern with any desired angle during the second SSL process. For example, a diamond-shaped grid pattern obtained with 45° rotation at the second PS pattern step is shown in Figure 2g. Further, 3-directional gold line patterns could be fabricated with grid shapes in the same *z*-axis space by repeating the SSL process three times (Figure 2h).

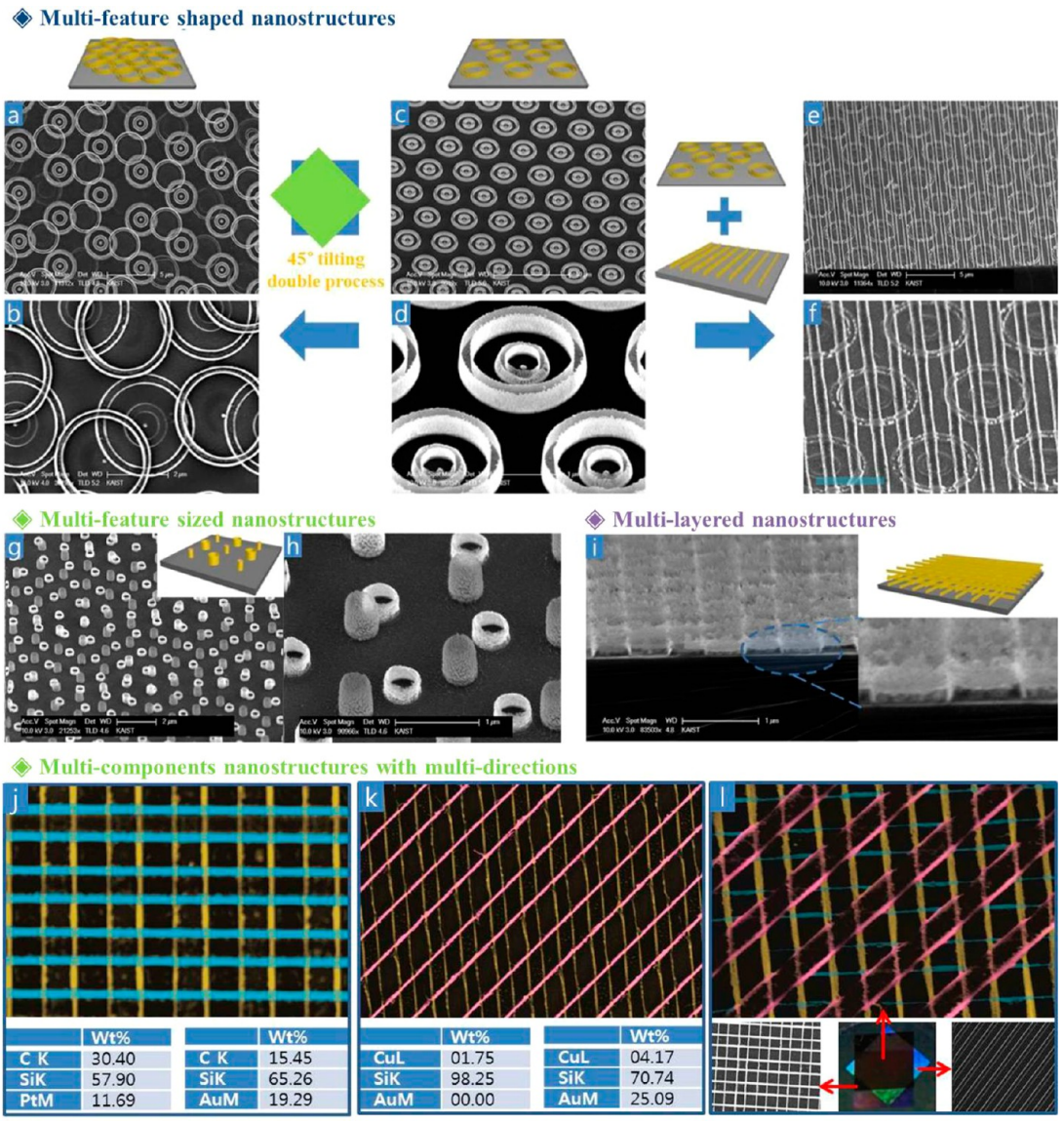

Figure 3. SEM images for fabrication of multifeature shaped (a–f)/multisized (g,h)/multilayered (i) 3-dimensional nanostructures, and false-colored SEM images and EDX data of multimetallic grid patterns with three different materials (j–l) and photoimage of patterned substrate (below center of part i) by repetitive secondary sputtering lithography. (c,d) A concentric ring shaped gold pattern with 15 nm width, 300 nm height, and ~2 nm diameter. (a,b) Olympic ring-shaped gold pattern where ring-shaped nanostructures were interconnected with each other in the same *z*-direction and (e,f) interconnected line-concentric ring merging patterned structures. (g,h) The two types of sub-20 nm width hole-cylinder patterns with different sizes in the same plane and (i) double layered nanopattern. (j–l) The SEM images of the grid pattern with 2 directions composed of Au and Pt (j), Au and Cu (k), and the SEM image of the 3-directional grid pattern that is composed of three different materials: Au, Pt, Cu (l).

Third and fourth steps can be performed to generate more complex nanopatterns.

A variety of complex 3D patterns can be easily fabricated using this method, provided that the components, shapes, and sizes of PS patterns are controlled by varying the fabrication conditions (Figure 3). For example, large concentric ring-shaped patterns with high resolution ~15 nm width were fabricated from a microsized concentric PS pattern (Figure 3c,d). The outermost large ring patterned nanostructure we have prepared thus far is 15 nm wide, 300 nm high, with a 2 μm diameter; the innermost ring is 15 nm wide, 300 nm high, with a 400 nm diameter. By using the multistep SSL technique, interconnected Olympic ring-shaped gold patterns could be prepared in the same *z*-direction (Figure 3a,b). In addition, interconnected line-concentric ring merging patterned structures were fabricated successfully from an identical microsized concentric PS pattern (Figure 3e,f). We also fabricated different sized and shaped nanopatterns from a single pillar master pattern which was composed of different feature shapes and dimensions on the substrate (Figure 3g,h). The control of the RIE conditions and PS thickness at each step of the SSL resulted in different

sizes of gold-hole cylinder patterns. Two hole-cylinder patterns with different feature shapes and dimensions were arranged regularly in a substrate plane: (i) 15 nm width, 500 nm height, and 450 nm diameter (gray color in Figure 3h) and (ii) 15 nm width, 230 nm height, and 460 nm diameter (white color in Figure 3h). The smaller hole-cylinder pattern was created with a 120 nm PS coating and low vacuum RIE for 90 s, while the taller hole cylinder pattern was fabricated with 300 nm PS coating and high vacuum RIE for 210 s. We enabled highly regular multilayered nanostructures by modifying the multistep SSL process, in which the PS residual layer was removed only until the top of the initial gold line was exposed by RIE, not the complete substrate, in the steps shown in Figure 1d,e. Then, gold deposition, ion-milling, and polymer removal were carried out in sequence, resulting in a double layer line pattern. A perpendicular line pattern was fabricated above the first line pattern with ~150 nm height, showing the stacking of the nanostructures (Figure 3i).

Importantly, this multistep SSL approach is very useful for fabricating ~10 nm scale multicomponent nanopatterns by using the angular distribution of ion-bombardment, in which two or more kinds of material are arranged alternately in the designated direction (Figure 3j–l). Indeed, multicomponent nanopatterns with ultrahigh resolution can control the electrical/optical properties and surface area of each material, enabling important applications such as two resistor-based biodetection, SERS-based biosensors, and nanoelectronics. We have fabricated multicomponent line patterns with different directions in a substrate surface by simply varying target materials with different directions in sequence (Supporting Information Figure S7). False-colored SEM images and their corresponding energy dispersive X-ray spectroscope (EDX) data show that the multimetallic grid pattern with a platinum (Pt, horizontal direction (*x*)) line pattern, a gold line pattern (perpendicular to Pt (*y*-directional)), and a copper (Cu, diagonal direction) line pattern were generated with high resolution (sub 20 nm) and high aspect ratio by utilizing the multistep SSL approach (Figure 3j–l). The spacing of adjacent parallel lines is ~500 nm, which is consistent with the spacing of a line master mold that has a 500 nm width and spacing dimensions. The images of Figure 3j,k represent multicomponent patterns of Pt (*x*-directional blue line)/Au (*y*-directional yellow line), and Au (*y*-directional yellow line)/Cu (diagonal red line) in a substrate, respectively. These were further identified by EDX. All of these metallic line patterns were generated from a single line-shaped master pattern. The below center area of the photoimage in Figure 3l corresponds to the SEM image of Figure 3l, that is, a line pattern with three different components of Au, Pt, Cu and three different directions. The overlapped areas explained above can be controlled by varying imprinted angles and positions.

To show the structural novelty and effectiveness of our method, we prepared a 15 nm scale ITO square grid pattern with an aspect ratio of ~20 for potential applications in liquid crystal displays (LCDs), touch screens, organic solar cells, and other opto-electronic devices. The ITO grid pattern fabricated by our multistep SSL technique has several significant advantages: it maintains electrical and optical properties, since the patterning method enables us to fabricate high nanostructures with ~300 nm height from only 20–30 nm etching of the ITO layer. Also, the patterned substrate can increase the surface area without optical hindrance due to high aspect ratio 15 nm pattern. We applied the grid nanopatterned ITO substrate to vertically align liquid crystal molecules, which is important for vertical alignment (VA) mode LCDs in the absence of any polymer alignment layers.

Figure 4a–c illustrates the overall procedure for the fabrication of LC cells with grid ITO patterned substrates. As briefly explained, as the high resolution lines with high aspect ratio cross each other, the increasing elastic energy density overcomes the surface anchoring of the line pattern, resulting in homeotropic alignment (see Supporting Information Figure S4). Figure 4d shows atomic force microscope (AFM) images of a highly periodic ITO grid pattern. White lines and dark regions in the AFM image represent thin ITO line structures and a flat ITO surface, respectively, confirming that highly uniform ITO grid patterns were successfully created over the entire surface area (5 mm × 5 mm). Height profiles from the AFM image show the generation of highly uniform thin walls that have a height of ~170 nm and aspect ratio of ~12. The conductivity of the ITO layer with the nanopattern on its surface is not much different from that of the pristine ITO layer due to the small decrease (~30 nm) in thickness during ion-bombardment. The sheet resistance of the ITO layer before and after nanopatterning are 8.2 ohm/square and 10 ohm/square. It is found that the electric conductance of patterned ITO did not decrease significantly, since the high aspect ratio ITO grid pattern with ~300 nm height can be made from ~30 nm etching of ITO by the SSL technique (see Supporting Information Figure S5). The photospectrometer results show that the transmittance of patterned ITO layer (90% at 550 nm) is almost the same as that of pristine ITO (90% at 550 nm). These results show that the ITO grid pattern with high resolution and high aspect ratio can be fabricated without decreasing the electrical/optical properties of the ITO layer (see Supporting Information Figure S5). We assembled the LC cell in vertical alignment mode by using two pieces of grid-patterned ITO glass in the absence of any polymer alignment layer. First, a nematic LC in the isotropic phase having negative dielectric anisotropy which aligns orthogonal to the applied electric field was injected into cells with a 2 μm gap. The assembled

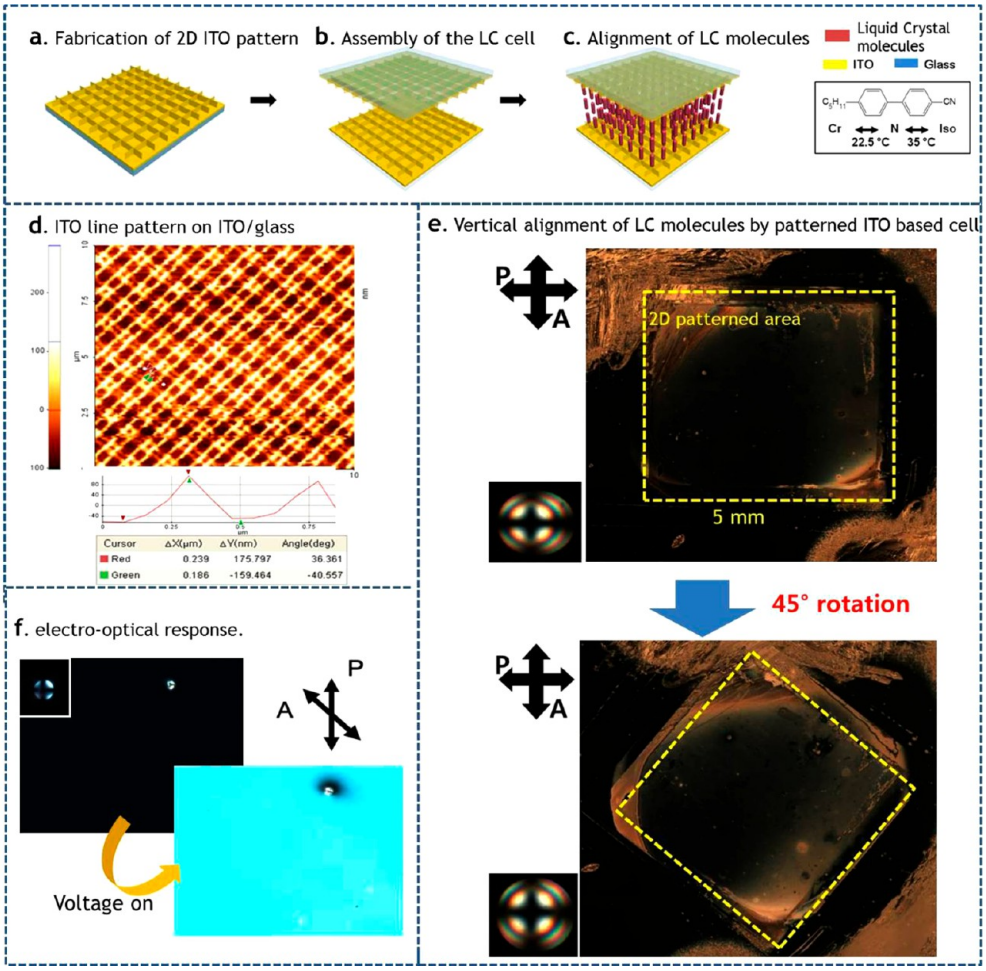

Figure 4. Vertical alignment (VA) of liquid crystal (LC) molecules using grid patterned ITO glass for LC-based display devices utilizing VA mode without an alignment layer. (a−c) The schematic illustration of the LC cell assembly using two-grid patterned ITO glass and (d) AFM image of grid patterned ITO surface and its line-cut analysis. (e) Wide view polarized optical microscope (POM) images for the vertical (homeotropic) alignment of LC molecules by grid patterned ITO topography and (f) POM images before and after applying an electric field to pristine and grid-patterned ITO glass.

cells are inspected by a polarized optical microscope (POM, Nikon, LV-100POL) equipped with a rotation stage in the plane perpendicular to the direction of light propagation. Figure 4e shows wide view POM images of the vertical cell. In this sample, both substrates possess 2D grid patterns with 15 nm width, 170 nm height, and 500 nm period in a 5 mm × 5 mm area, as marked in the figure. The yellow broken lines in the central portion of the images correspond to the patterned area of the substrate. As clearly seen in the POM images, the texture in the patterned area has a dark appearance (top image in Figure 4e) and retains its dark texture upon rotation of the cell by 45° (bottom image in Figure 4e), indicating that the optical axis of LCs in the patterned area coincides with the direction of light propagation. We employed a Bertland lens with a 100× objective to conduct conoscopic observations of interference patterns. The conoscopic interference pattern consisted of a centered black cross superimposed on circular bands of interference colors observed for homeotropic anchoring (inset of Figure 4e). It has been well demonstrated that these types of interference features arise from homeotropically aligned molecules where the optical axis emerges when observed by conoscopy. The interference pattern remains the same upon rotating the samples (inset of Figure 4h), clearly showing that the optical axis of the LC cell is normal to the substrate. On the basis of POM and conoscopic observations, we confirmed that the topographical anisotropy of 2D grid ITO patterns can efficiently induce a good, uniform, and homeotropic alignment of the LC director. From a series of electro-optic experiments, we confirmed that the homeotropic alignment of LCs in cell were changed and retained when the electric field was on/off (Figure 4f). This phenomenon shows our grid patterns actually induce homeotropic alignment of LCs. Unfortunately, the response time (rising time 30−40 ms and 60−70 ms) of our LC cell we obtained was 90−100 ms, which is slower than the conventional vertical alignment LC cell based on polymer alignment layer. This is attributed to low anchoring energy of our grid pattern

for LCs, leading to deterioration of falling time. However, it is expected that the anchoring energy can be enhanced by fabricating more dense (line pitch) and higher pattern structures. There are several papers by Yokoyama and Noel Clark groups that report anchoring of nematic liquid crystals on a two-dimensionally grooved surface.[31,35] Depending on aspect ratio (width/depth ratio) of pattern, the surface can exhibit bistable anchoring or homeotropic anchoring. When the patterns are wide and shallow, the elastic distortion of a liquid crystal adjacent to the surface leads to a bistable distorted planar state with the average director orientation along a diagonal of the square.[32−34] Yi et al. demonstrated topographic-pattern-induced homeotropic alignment of nematic liquid crystals by using deep nanoscale arrays of square wells.[31] According to their theory, the elastic energy density increases as the spatial gradients of the director field increase due to narrow width and deep depth of the well until it exceeds the planar surface anchoring energy. At this point, the bottom of the well goes homeotropic. The homeotropic alignment induced by grid ITO line patterns in our study can be understood in this way even though the dimension is somewhat different. In addition, it should be noted that the quasihomeotropic state suggested by their simulation results is consistent with our POM observation. As shown in Figure 4, the texture on patterned area is not completely dark, indicating a spatial gradient of the tilt angle. On the other hand, the nonpatterned area shows complete extinction because there is no distorted nematic director field induced by patterns.

CONCLUSIONS

In summary, we have described a valuable new approach to the fabrication of high resolution (∼15 nm) 3D patterns of multiple shapes, dimensions, and materials, with a high aspect ratio over large areas, using advanced repetitive secondary sputtering lithography (SSL). SSL attaches target materials to the side surfaces of prepatterned polymers fabricated during accelerated Ar ion-assisted bombardment. In developing beyond the previous SSL method, continuous and more complex patterns with 10 nm resolution were generated by combining the isolated patterns from microsized single master mold patterns. In addition, in the case of the SSL patterning of commercial ITO layers, grid-patterned ITO glass can simultaneously function as a LC alignment layer and transparent electrode. It is expected that the 10 nm scale 3D patterns with different materials and different features/sizes enables a wide range of electrical/optical applications of the technique to nanoelectronics, energy devices, biosensors, and display devices. Accordingly, the new lithographic method will serve as a new technique for fabricating complex nanoscale patterns with multiple shapes, dimensions, and materials.

METHODS

Preparation of Mold Pattern. The PDMS mold was replicated from a silicon master with a 600 nm depth. First, hard PDMS which supports the structure of the master was produced by mixing trimethylsiloxy-terminated vinylmethyl-siloxane-dimethylsiloxane copolymers, 2,4,6,8-tetramethyl tetravinyl-cyclotetrasiloxane, Pt-divinyl-tetramethylsiloxane, trimethylsiloxy-terminated methylhydrosiloxane, and dimethylsiloxane copolymers. Then spin coating of the mixture onto the silicon master was carried out immediately after mixing at 2000 rpm, 25 s and procured for 10 min at 60 °C. Soft PDMS was then prepared by mixing the PDMS prepolymer for 10 min at 60 °C. Then soft PDMS was prepared by mixing the PDMS prepolymer (Sylgard 184 A/B = 10:1, Dow Corning) and then pouring the mixture onto the hard PDMS layer. After bubbles came out from the mixture, it was cured at 80 °C for 2 h.

Preparation of Interconnected Complex 3D Gold Pattern by Repetitive Secondary Sputtering Lithography. An array of line shapes (pitch size, 500 nm; height, 600 nm; area, 5 mm × 5 mm) and circle-shaped pillars (diameter, 500 nm; height, 600 nm,) in silicon was prepared with e-beam lithography. A highly uniform gold layer (30 nm gold/2 nm Cr) was deposited on a silicon wafer by e-beam evaporation. The gold coated substrate was coated with 1−8 wt % polystyrene (PS, 18 000 g mol^{-1}, Sigma Aldrich) in toluene for 45 s at 3000 rpm. Then the cured PDMS mold with topographic features was placed onto the polymer film. After heating at 135 °C for 60 min and cooling to room temperature, the mold was removed from the surface. After removing the replica mold, a PS nanopattern was formed on the substrate and acted as a framework during the ion-bombardment process. The PS prepattern was removed by reactive ion etching (RIE) using a mixture of O_2 (40 sccm) and CF_4 (60 sccm) plasma at a chamber pressure of 20 mTorr and a power density of 80 W. Then the gold layer was simultaneously etched and deposited onto the side surface of the PS pattern using secondary sputtering during ion bombardment, and 10 nm gold nanopatterns were formed on the substrate. To make a second 3D gold pattern by second secondary sputtering lithography, the gold patterned substrate was coated with 8 wt % polystyrene (PS, 18 000 g mol^{-1}, Sigma Aldrich) in toluene for 45 s at 3000 rpm. The PS concentration is relatively high since the spin-coated PS thickness should be thick enough to cover the initial gold pattern completely. Then the cured PDMS mold with topographic features was placed onto the polymer film perpendicular to the initial line pattern. After heating at 135 °C for 60 min and cooling to room temperature, the mold was removed from the surface. After removing the replica mold, a PS nanopattern was formed on the substrate and acted as framework during the etching process. In order to anisotropically etch the thick PS layer without decreasing of width of PS, the thick PS prepattern was removed by high vacuum reactive ion etching (RIE) using a mixture of O_2 (40 sccm) and CF_4 (60 sccm) plasma at a chamber pressure of 20 mTorr and a power density of 80 W. Then the gold layer was simultaneously etched and deposited onto the side surface of the PS pattern using secondary sputtering during ion bombardment. PS residual layers in the gold pattern were clearly removed by RIE O_2 100 sccm.

LC Cell Fabrication Using Patterned ITO Substrates. Electro-optic LC cells were fabricated by assembling ITO glass possessing ITO square grid patterns. The cell thickness was controlled using microbead spacers, and the cells were sealed by a UV-curable adhesive (NOA 63, Norland Product Inc., Cranbury, NJ). The fabricated empty cell was placed on a temperature-controlled hot plate (FP82HT Mettler Toledo Korea, Seoul, Korea), and 5CB

was loaded by capillary action at 40 °C in the isotropic phase. After the filling process, the cell was cooled to room temperature at a rate of 2 °C min^{-1}.

Characterization. SEM (Sirion FE-SEM, FEI, NNFC in KAIST) images were obtained by the collection of secondary electrons produced by bombarding the sample with an acceleration voltage between 3 and 10 kV. Surface topological measurements were performed under ambient conditions using a commercial AFM (SPA400, Seiko, Japan) equipped with a 100 mm × 100 nm scan head. LC alignment was probed using polarized optical microscopy. Electric conductance and optical transmittance of the patterned ITO substrate were measured using a probe station (4200-SCS Keithley, Keithley Instruments, Inc., Cleveland, OH) and UV/vis absorption spectroscopy (92-570, JASCO, Tokyo, Japan) was used to determine optical properties.

Conflict of Interest: The authors declare no competing financial interest.

Supporting Information Available: Schematic images for secondary sputtering phenomenon during ion-bombardment process, SEM images that support the secondary sputtering lithography method, SEM images for fabrication of various multifeature shaped/multisized 3-dimensional nanostructures by repetitive secondary sputtering lithography, and mechanism for homeotropic (vertical alignment, VA) LC molecules alignment by square grid ITO pattern with 10 nm ultra high resolution. This material is available free of charge *via* the Internet at http://pubs.acs.org.

Acknowledgment. This research was supported by National Research Foundation of Korea (NRF) grant funded by the Ministry of Science, ICT and Future Planning, Korea (MSIP, NRF-2012R1A2A1A01003537) and Global Frontier Grant funded by center for Advanced Soft Electronics under the Global Frontier Research Program of the Ministry of Science, ICT and Future Planning, Korea (MSIP, Grant NRF-2012M3A6A5055744). SEM experiments were carried out at NNFC in KAIST.

REFERENCES AND NOTES

1. Kim, D.-H.; Lu, N.; Ghaffari, R.; Rogers, J. A. Inorganic Semiconductor Nanomaterials for Flexible and Stretchable Bio-Integrated Electronics. *NPG Asia Mater.* **2012**, *4*, e15.
2. Catrysse, P. B.; Fan, S. Nanopatterned Metallic Films for Use as Transparent Conductive Electrodes in Optoelectronic Devices. *Nano Lett.* **2010**, *10*, 2944–2949.
3. Jeon, H.-J.; Baek, Y. -K.; Yang, S. B.; Lee, S.-K.; Jung, J.-M.; Jung, H.-T. Patterned Nano-Sized Gold Dots Within FET Channel: From Fabrication to Alignment of Single Walled Carbon Nanotube Networks. *J. Mater. Chem.* **2011**, *21*, 14285–14290.
4. Wu, W.; Cheng, L.; Bai, S.; Wang, Z. L.; Qin, Y. Directional Transport of Polymer Sheet and a Microsphere by a Rotationally Aligned Nanowire Array. *Adv. Mater.* **2012**, *24*, 817–821.
5. Soleymani, L.; Fang, Z.; Sargent, E. H.; Kelley, S. O. Programming the Detection Limits of Biosensors Through Controlled Nanostructuring. *Nat. Nanotechnol.* **2009**, *4*, 844–848.
6. Calleja, M.; Kosaka, P. M.; Paulo, A. S.; Tamayo, J. Challenges for Nanomechanical Sensors in Biological Detection. *Nanoscale* **2012**, *4*, 4925–4938.
7. Chae, S. S.; Min, H.; Lee, J. H.; Hwang, B.; Sung, W. M.; Jang, W. S.; Yoo, Y. B.; Oh, J.; Park, J. H.; Kang, D.; *et al.* Fabriation of a Multidomain and Ultrafast-Switching Liquid Crystal Alignment Layer Using Contact Printing with a Poly(dimethylsiloxane) Stamp. *Adv. Mater.* **2013**, *25*, 1408–1414.
8. Livneh, N.; Strauss, A.; Schwarz, I.; Rosenberg, I.; Zimran, A.; Yochelis, S.; Chen, G.; Banin, U.; Paltiel, Y.; Rapaport, R. Highly Directional Emission and Photon Beaming from Nanocrystal Quantum Dots Embedded in Metallic Nanoslit Arrays. *Nano Lett.* **2011**, *11*, 1630–1635.
9. Mann, S. Self-Assembly and Transformation of Hybrid Nano-Objects and Nanostructures under Equilibrium and Non-Equilibrium Conditions. *Nat. Mater.* **2009**, *8*, 781–792.
10. Lee, J.; Lee, S. K.; Jung, J.-M.; Baek, Y.-K.; Jung, H.-T. Fabrication of Highly Ordered Multi-Segment Line Pattern over a Large-Area. *RSC Adv.* **2012**, *2*, 2043–2046.
11. Pradhan, S.; Ghosh, D.; Chen, S. Janus Nanostructures Based on Au-TiO_2 Heterodimers and Their Photocatalytic Activity in the Oxidation of Methanol. *ACS Appl. Mater. Interfaces* **2009**, *1*, 2060–2065.
12. Peroz, C.; Dhuey, S.; Cornet, M.; Vogler, M.; Olynick, D.; Cabrini, S. Single Digit Nanofabrication by Step-and-Repeat Nanoimprint Lithography. *Nanotechnology* **2012**, *23*, 015305.
13. Lucas, B. D.; Kim, J.-S.; Chin, C.; Guo, L. J. Nanoimprint Lithography Based Approach for the Fabrication of Large-Area, Uniformly Oriented Plasmonic Arrays. *Adv. Mater.* **2008**, *20*, 1129–1134.
14. Lee, S.-K.; Jung, J.-M.; Lee, J.; Jung, H.-T. Fabrication of Complex Patterns with a Wide Range of Feature Sizes from a Single Line Prepattern by Successive Application of Capillary Force Lithography. *Langmuir* **2010**, *26*, 14359–14363.
15. Gates, B. D.; Xu, Q.; Stewart, M.; Ryan, D.; Wilson, C. G.; Whitesides, G. M. New Approaches to Nanofabrication: Molding, Printing, and Other Techniques. *Chem. Rev.* **2005**, *105*, 1171–1196.
16. Geissler, M.; Xia, Y. Patterning: Principles and Some New Developments. *Adv. Mater.* **2004**, *16*, 1249–1269.
17. Odom, T. W.; Thalladi, V. R.; Love, J. C.; Whitesides, G. M. Generation of 30−50 nm Structures Using Easily Fabricated, Composite PDMS Masks. *J. Am. Chem. Soc.* **2002**, *124*, 12112–12113.
18. Zhao, Y.; Jansen, H.; Boer, M. D.; Berenschot, E.; Bouwes, D.; Girones, M.; Huskens, J.; Tas, N. Combining Retraction Edge Lithography and Plasma Etching for Arbitrary Contour Nanoridge Fabrication. *J. Micromech. Microeng.* **2012**, *20*, 095022.
19. Li, Z.; Liu, P.; Liu, Y.; Chen, W.; Wang, G. Fabrication of Size-Controllable Fe_2O_3 Nanoring Array *via* Colloidal Lithography. *Nanoscale* **2011**, *3*, 2743–2747.
20. Kravchenko, A.; Shevchenko, A.; Ovchinnikov, V.; Priimagi, A.; Kaivola, M. Optical Interference Lithography Using Azobenzene-Functionalized Polymers for Micro- and Nanopatterning of Silicon. *Adv. Mater.* **2011**, *23*, 4174.
21. Xu, Q.; Rioux, R. M.; Dickey, M. D.; Whitesides, G. M. Nanoskiving: A New Method to Produce Arrays of Nanostructures. *Acc. Chem. Res.* **2008**, *41*, 1566–1577.
22. Kim, P.; Epstein, A. K.; Khan, M.; Zarzar, L. D.; Lipomi, D. J.; Whitesides, G. M.; Aizenberg, J. Structural Transformation by Electrodeposition on Patterned Substrates (STEPS): A New Versatile Nanofabrication Method. *Nano Lett.* **2012**, *12*, 527–533.
23. Utke, I.; Hoffmann, P.; Melngailis, J. Gas-Assisted Focused Electron Beam and Ion Beam Processing and Fabrication. *J. Vac. Sci. Technol. B* **2008**, *26*, 1197–1276.
24. Fischer, A. C.; Belova, L. M.; Ricker, Y. G. M.; Malm, B. G.; Radamson, H. H.; Kolahdouz, M.; Gylfason, K. B.; Stemme, G.; Niklaus, F. 3D Free-Form Patterning of Silicon by Ion Implanation, Silicon Deposition, and Selective Silicon Etching. *Adv. Mater.* **2012**, *22*, 4004–4008.
25. Jeon, H.-J.; Kim, K. H.; Baek, Y.-K.; Kim, D. W.; Jung, H.-T. A New Top-Down Approach for Fabrication High-Aspect-Ratio Complex Nanostructures with 10 nm-Scale Features. *Nano Lett.* **2010**, *10*, 3604–3610.
26. Jeong, H. S.; Jeon, H.-J.; Kim, Y. H.; Oh, M. B.; Kumar, P.; Kang, S.-W.; Jung, H.-T. Bifunctional ITO Layer with a High Resolution, Surface Nano-Pattern for Alignment and Switching of LCs in Device Applications. *NPG Asia Mater.* **2012**, *4*, e7.
27. Jeon, H.-J.; Yoo, H.-W.; Lee, E. H; Jang, S. W.; Kim, J. -S.; Choi, J. K.; Jung, H.-T. Fabrication of Complex 3-Dimensioanl Patterned Structures on a ∼10nm Scale from a Single Master Pattern by Secondary Sputtering Lithography. *Nanoscale* **2013**, *5*, 2358–2363.

28. Zhao, D.; Huang, W.; Cao, H.; Zheng, Y.; Wang, G.; Yang, Z.; Yang, H. Homeotropic Alignment of Nematic Liquid Crystals by a Photocross-Linkable Orgarnic Monomer Containing Dual Photofunctional Groups. *J. Phys. Chem. Lett. B* **2009**, *113*, 2961–2965.
29. Liu, B.-Y.; Chem, L.-J. Role of Surface Hydrophobicity in Pretilt Angle Control of Polymer-Stabilized Liquid Crystal Alignment System. *J. Phys. Chem. C* **2013**, *117*, 13474–13478.
30. Hwang, B. H.; Ahn, H. J.; Rho, S. J.; Chae, S. S.; Baik, H. K. Vertical Alignment of Liquid Crystals with Negative Dielectric Anisotropy on an Inorganic Thin Film with a Hydrophilic Surface. *Langmuir* **2009**, *25*, 8306–8312.
31. Yi, Y.; Lombardo, G.; Ashby, N.; Barberi, R.; Maclennan, J. E.; Clark, N. A. Topographic-Pattern-Induced Homeotropic Alignment of Liquid Crystals. *Phys. Rev. E* **2009**, *79*, 041701.
32. Gwag, J. S.; Kim, J.-H.; Yoneya, M.; Yokoyama, H. Surface Nematic Bistability at Nanoimprinted Topography. *Appl. Phys. Lett.* **2008**, *92*, 153110.
33. Yi, Y.; Nakata, M.; Martin, A. R.; Clark, N. A. Alignment of Liquid Crystals by Topographically Patterned Polymer Films Prepared by Nanoimprint Lithography. *Appl. Phys. Lett.* **2007**, *90*, 163510.
34. Yi, Y. W.; Khire, V.; Bowman, C. N.; Maclennan, J. E.; Clark, N. A. Organization of Liquid Crystals on Submicron Scale Topographic Patterns with Fourfold Symmetry Prepared by Thiolene Photopolymerization-Based Nanoimprint Lithography. *J. Appl. Phys.* **2008**, *103*, 093518.
35. Fukuda, J.-I.; Gwag, J. S.; Yoneda, M.; Yokoyama, H. Theory of Anchoring on a Two-Dimensionally Grooved Surface. *Phys. Rev. E* **2008**, *77*, 011702.